Crystal structure of $Li_x Ni_{2-x}O_2$ and a lattice-gas model for the order-disorder transition

W. Li, J. N. Reimers, and J. R. Dahn

Department of Physics, Simon Fraser University, Burnaby, British Columbia, Canada V5A 1S6

(Received 30 December 1991; revised manuscript received 10 March 1992)

The crystal structure of $Li_x Ni_{2-x}O_2$ for $0 \leq x \leq 1$ is reported. For $x < 0.62$, $Li_x Ni_{2-x}O_2$ has a disordered rocksalt structure. For $0.62 \leq x \leq 1.0$, Li and Ni atoms segregate into Li-rich and Ni-rich layers normal to one of the four $\langle 111 \rangle$ directions in the cubic lattice. This breaks the cubic symmetry and an apparently continuous transition to a hexagonal phase occurs. At $x = 1$, alternate cation layers are nearly pure Li and pure Ni. The degree of order is quantified by defining an order parameter η, which we take to be the difference in the Li composition of neighboring metal atom layers. Using x-ray diffraction and Rietveld profile refinement, we have measured η versus x. We model $Li_x Ni_{2-x}O_2$ as a lattice of oxygen atoms into which cations (either Li or Ni) can be inserted, subject to the constraint that the number of cations equals the number of oxygen atoms. Interactions between cations on nearest- and on next-nearest-neighbor sites are included, and the lattice-gas model is solved with use of mean-field and Monte Carlo methods. We find that the nearest-neighbor interaction is not sensitive to the observed ordering and that we can describe the experimental variation of η versus x for an appropriate choice of the next-nearest-neighbor interaction.

I. INTRODUCTION

NiO has the rock-salt structure. Li-Ni-O compounds usually have one oxygen atom per metal atom and are normally based on layers of closed-packed oxygen atoms. A technique to prepare $LiNiO_2$ has been developed by Dyer *et al.*[1] Goodenough *et al.*[2,3] and Bronger *et al.*[4] studied the phases in the solid solution series $Li_x Ni_{2-x}O_2$ $(0 < x < 1)$. They showed that a disordered rock-salt-type structure exists for $x < 0.56$ and partial cation ordering occurs for $x > 0.6$. They suggested that there is an ordering of the cations in alternate $(111)_C$ [(111) in the cubic structure] planes and calculated the order parameter as a function of x based on the magnetic measurements and the analysis of the x-ray diffraction patterns.

Rechargeable batteries can be made using two different intercalation compounds as the electrodes. $LiNiO_2$ is now one of the possible choices for the cathode.[5,6] We have learned that the performance of the cells depends on the stoichiometry of $Li_x Ni_{2-x}O_2$ used in the cell. Ni atoms enter the Li layers and presumably these Ni atoms impede the diffusion of Li. Therefore, it is important to know how much Ni enters the Li layers as a function of x. We undertook the work described here because there has not been a careful structural study on this solid solution.

To our knowledge $Li_x Ni_{2-x}O_2$ can only be made in powder form. Therefore structural information is best obtained using profile refinement methods.[7] The Rietveld structure refinement procedure obtains a least-squares fit between the calculated and observed profile intensities and is now well established.[8] In x-ray Rietveld analysis, the best fit is obtained by adjusting cell constants, atomic coordinates, site occupancies, the peak shape, the background, etc. This method is used here to analyze the powder-diffraction profiles of $Li_x Ni_{2-x}O_2$.

Our structural results agree with those previously reported, but are more quantitative. The order-disorder transition at $x = 0.62$ has been modeled with a lattice-gas model. The model describes the data well.

II. SAMPLE PREPARATION

$Li_x Ni_{2-x}O_2$ samples were prepared by reacting stoichiometric mixtures of $LiOH \cdot H_2O$ and $Ni(OH)_2$. The powders were ground with a mortar and pestle and were then heated at 700 °C for 2 h in air followed by slow cooling over several hours to room temperature. LiOH reacts rapidly with NiO [which forms when $Ni(OH)_2$ decomposes around 300 °C] which minimizes Li loss due to extended heating which commonly occurs when Li_2CO_3 is used as a starting material. X-ray diffraction measurements were made using a Phillips powder diffractometer with a diffracted beam monochromator. We used Cu $K\alpha$ radiation for the measurements described here. Single phase $Li_x Ni_{2-x}O_2$ was easily made for $0 \leq x \leq 1$. Li_2CO_3 appeared when the [Li]:[Ni] ratio was more than 1. This could be avoided if the reaction was carried out under O_2 (Li_2O forms instead), but still we could not prepare single-phase materials with $x > 1$.

III. STRUCTURE AND ORDER PARAMETER

The compounds $Li_x Ni_{2-x}O_2$ are structurally related to NiO which has the rock-salt structure with $a_c = 4.168$ Å. In this structure, the metal ions occupy one face-centered cubic (fcc) frame while the oxygen ions occupy the other fcc frame. These two fcc frames are shifted by $a_c/2$ along one of the three cubic axes. For $0.0 \leq x < 0.62$ $Li_x Ni_{2-x}O_2$ is cubic and for $0.62 \leq x \leq 1.0$ it is hexagonal. Figure 1(a) shows the metal atom positions when $x = 1$ and c_h and a_h are cell constants in the hexagonal
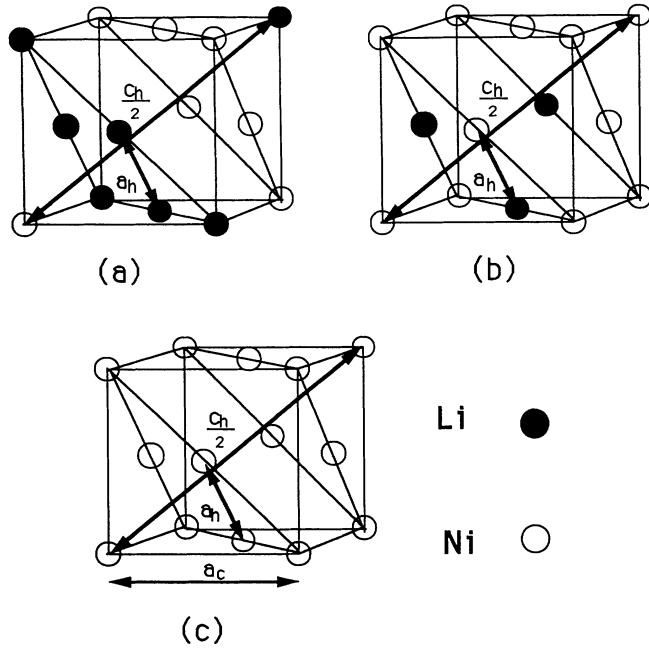
FIG. 1. Metal positions in Li$_x$Ni$_{2-x}$O$_2$. (a) $x=1.0$ and $\eta=1.0$, LiNiO$_2$ with the perfect ordered structure. (b) $0<x<1$ and $0<\eta<1$ with the partial ordered structure. (c) $x=0.0$ and $\eta=0.0$, NiO.

structure. When $c_h/a_h=2\sqrt{6}$ the unit cell is equivalent to the cubic one with $a_c=\sqrt{2}\,a_h$.

As Fig. 1(a) shows, the metal atoms segregate into predominantly Li-filled layers (L layers) and predominantly Ni-filled layers (N layers) near $x=1$. As x in Li$_x$Ni$_{2-x}$O$_2$ decreases, Ni atoms must move into the L layers and Li atoms may move into N layers. We define a long-range order parameter as

$$\eta=|\langle x_L\rangle-\langle x_N\rangle|\ ,\tag{1}$$

where

$$\langle x_L\rangle+\langle x_N\rangle=x\tag{2}$$

and where $\langle x_L\rangle$ and $\langle x_N\rangle$ are the average Li concentrations in the L layers and N layers, respectively. In Fig. 1(a), $\eta=1$ since the structure is perfectly ordered. Figure 1(b) shows a situation for $x<1$ where the lattice is partially ordered and has $\eta<1$. Finally, Fig. 1(c) shows the cation positions in NiO which has $\eta=0$ according to our definition.

In our profile refinements we refine the concentrations x_L and x_N. In an L layer each site is filled by an average atom consisting of x_L Li and $(1-x_L)$ Ni. In an N layer, each site is filled by x_N Li and $(1-x_N)$ Ni. Since lithium only has three electrons we are most sensitive to lithium through the absence of Ni, since we assume the number of cations in the structure equals the number of oxygen atoms.

IV. REFINEMENT RESULTS

The basis of the Rietveld method[7–12] is the equation

$$Y_{ic}=Y_{ib}+\sum_k G_{ik}I_k\ ,\tag{3}$$

where Y_{ic} is the net intensity calculated at point i in the pattern and Y_{ib} is the background intensity. In our calculation, Y_{ib} was chosen as $A+B\theta+C/\theta$ and A, B, C are profile parameters. G_{ik} is a normalized peak profile function, it was chosen as a pseudo-Voigt function,[12] which is a mixture of Gaussian and Lorentzian peaks. I_k is the intensity of the kth Bragg reflection and k is summed over all reflections contributing to the intensity at point i.

The intensity I_k is given by the expression

$$I_k=SM_kL_k|F_k|^2W_k\ ,\tag{4}$$

where S is the usual scale factor, M_k is the multiplicity, L_k is the Lorentz polarization factor, F_k is the structure factor, and W_k is an isotropic Debye-Waller factor which we have assumed is the same for each atom in the unit cell.

Refinements were done in the space group $R\bar{3}m$, which is the space group for LiNiO$_2$. The least-squares procedures uses the Newton-Raphson algorithm to minimize the quantity

$$\chi^2=\sum w_i(Y_{i0}-Y_{ic})^2\ ,\tag{5}$$

where Y_{i0} is the set of observed diffraction intensities collected at each step across the pattern. w_i is the statistical weight assigned to each observation; we use $w_i=1/Y_{i0}$. One measure of the quality of our refinement is the Bragg R factor, R_B, defined as

$$R_B=\frac{\sum|I_{k0}-I_{kc}|}{\sum I_{k0}}\times 100\%\ ,\tag{6}$$

where I_{k0} is the observed integrated intensity of reflection k calculated at the end of the refinement after apportioning each Y_{i0} between the contributing peaks and background when that is refined according to the calculated
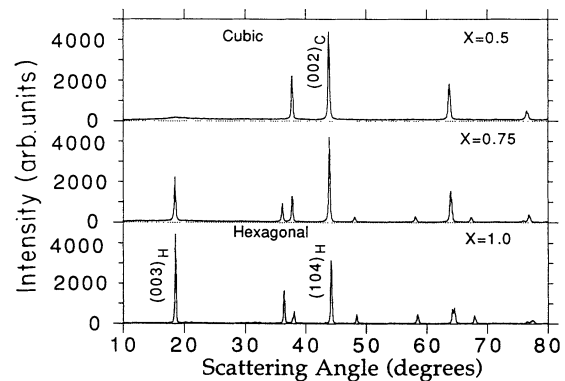

FIG. 2. X-ray diffraction patterns for three Li$_x$Ni$_{2-x}$O$_2$ samples with x as indicated in the figure. Miller indices for Bragg peaks referred to in the text are indicated.
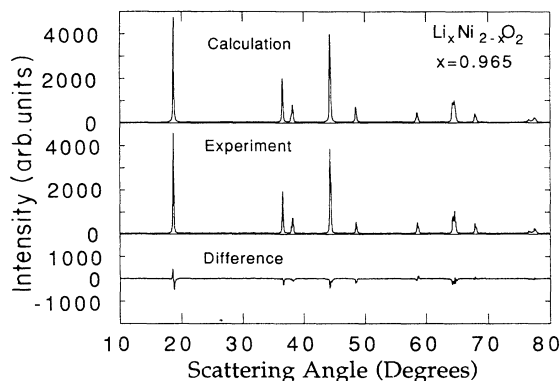
FIG. 3. Experiment and fitted profile for $Li_{0.965}Ni_{1.035}O_2$ as indicated in the figure. The difference between the two profiles is also shown.

FIG. 5. The cell constant, c_h, of the hexagonal structure vs "x from Rietveld profile fitting" in $Li_xNi_{2-x}O_2$.

intensities I_{kc}.

Figure 2 shows x-ray diffraction profiles for several $Li_xNi_{2-x}O_2$ samples, to show the changes in the profile which occur as x changes. The $(003)_H$ peak decreases in intensity as x decreases, becoming weak and broad below $x=0.62$, indicating short-range instead of long-range correlations. The sharp peak appears only when the average composition of the L and N layers differs. The ratio of the intensities of the $(101)_H$ and the $(102)_H$, $(006)_H$ peaks changes with x and has been previously used to estimate x in $Li_xNi_{2-x}O_2$.[5]

Figure 3 shows an example of a Rietveld profile refinement for one of our samples. For $x > 0.62$, the fits included at least 12 Bragg peaks while for $x < 0.62$ only 6 (including two peaks between 80° and 100° 2θ scattering angle) experimentally measured peaks could be used. For $x < 0.62$, the Rietveld program is unable to the fit the Broad short-range order peak well near $2\theta = 18.5°$, because its width does not follow the functional form used by the Rietveld method. Nevertheless, we refined the entire profile and considered the short-range order peak separately as we describe later. Table I reports the re-
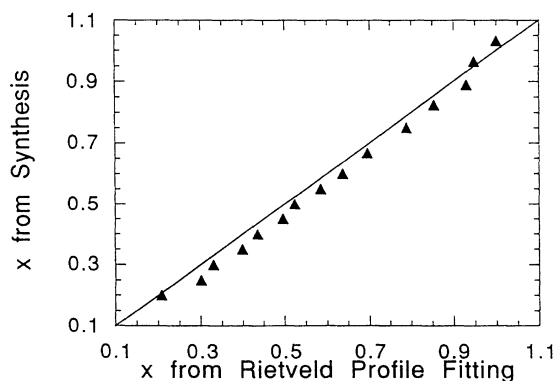
sults of our refinements. For all refinements, R_B, was less than 3.4%, indicating good agreement between the data and the structural model.

The composition of the samples are determined in two ways. First we simply use the mole ratios of the starting materials mixed in the synthesis. The Rietveld program gave the second value of x, obtained by summing x_N and x_L returned by the program. We call the first composition "x from synthesis" and the second "x from Rietveld profile fitting." Figure 4 shows that these compositions agree well with each other which gives us confidence in the quality of our samples and the refinement method. The solid line in Fig. 4 shows the line "x from synthesis"="x from Rietveld profile fitting." Apart from 2 points, our data fall systematically to one side of the line suggesting some small problem with our refinement methods or in the original stoichiometries of our starting materials. In what follows we plot refined qualities versus "x from Rietveld profile fitting" for consistency. Substituting for "x from synthesis" does not change the results significantly.

All Rietveld profile fitting is based on the hexagonal structure, even if the structure could be fitted by a cubic structure for $0.0 < x < 0.62$. The cell constants a_h and c_h in Figs. 5 and 6 are in good agreement with the data

FIG. 4. The composition of $Li_xNi_{2-x}O_2$ measured from mole ratios of reactants ("x from synthesis") plotted versus the composition determined from Rietveld profile analysis ("x from Rietveld profile fitting"). The solid line is "x from synthesis"="x from Rietveld profile analysis."
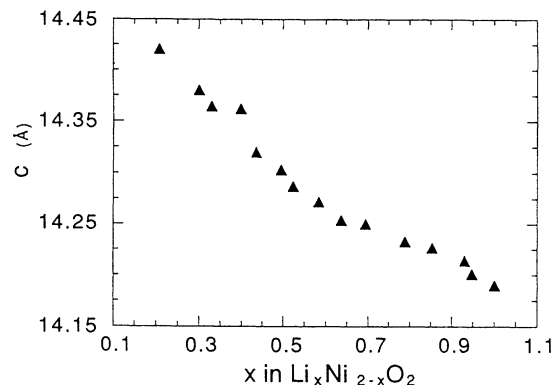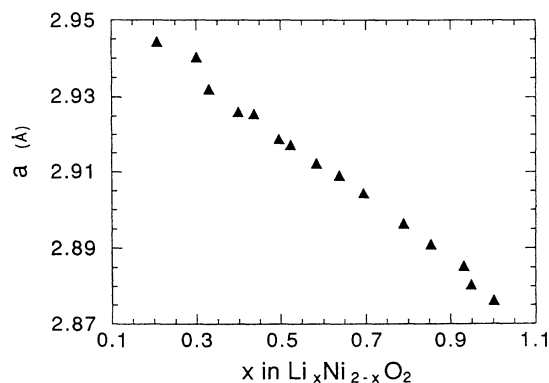

FIG. 6. The cell constant, a_h of the hexagonal structure vs "x from Rietveld profile fitting" in $Li_xNi_{2-x}O_2$.

TABLE I. Results of profile refinement for $Li_xNi_{2-x}O_2$ samples.

Sample No.	x^a	x^b	a_h (Å)	c_h (Å)	$O(z)$	x_L	x_N	η	R_{wp}	R_{expt}	R_B
1	1.032(1)	1.001(10)	2.8762(1)	14.190(1)	0.2581(3)	0.980(9)	0.021(3)	0.959(10)	14.1	8.9	3.00
2	0.965(1)	0.949(11)	2.8804(1)	14.201(1)	0.2559(3)	0.947(9)	0.002(6)	0.945(11)	12.8	9.7	3.36
3	0.889(1)	0.932(9)	2.8854(1)	14.213(1)	0.2579(3)	0.915(3)	0.017(8)	0.898(9)	14.2	9.1	2.35
4	0.824(1)	0.855(3)	2.8910(2)	14.227(2)	0.2571(3)	0.843(3)	0.012(1)	0.831(3)	13.6	9.0	2.26
5	0.750(1)	0.790(9)	2.8964(2)	14.234(2)	0.2568(3)	0.750(4)	0.040(8)	0.710(9)	12.8	9.1	2.43
6	0.667(1)	0.695(10)	2.9044(1)	14.250(1)	0.2571(3)	0.630(4)	0.065(9)	0.565(10)	11.5	9.2	2.92
7	0.600(1)	0.638(10)	2.9090(4)	14.254(4)	0.2573(4)	0.502(5)	0.136(9)	0.366(10)	12.5	6.7	2.10
8	0.550(1)	0.585(12)	2.9122(5)	14.272(4)	0.2560(5)	0.436(6)	0.148(10)	0.288(12)	12.9	6.7	1.96
9	0.500(1)	0.524(12)	2.9172(5)	14.287(5)	0.2554(8)	0.329(6)	0.195(10)	0.134(12)	9.92	3.4	1.39
10	0.450(1)	0.496(14)	2.9188(6)	14.303(6)	0.2538(1)	0.309(8)	0.188(11)	0.121(14)	15.8	10.2	1.31
11	0.400(1)	0.436(13)	2.9256(8)	14.320(7)	0.2561(5)	0.264(7)	0.172(11)	0.092(13)	15.8	10.5	1.52
12	0.350(1)	0.399(13)	2.9262(13)	14.362(13)	0.2553(10)	0.224(6)	0.175(11)	0.049(13)	7.93	5.0	0.90
13	0.300(1)	0.331(13)	2.9321(10)	14.365(8)	0.2547(11)	0.185(7)	0.146(11)	0.039(13)	15.8	10.2	1.52
14	0.250(1)	0.301(14)	2.9403(5)	14.380(5)	0.2542(10)	0.171(7)	0.130(12)	0.041(14)	6.69	5.0	1.07
15[c]	0.200(1)	0.208(11)	2.9444(2)	14.424(10)	Cubic	Cubic	Cubic	0	9.09	4.8	1.21

[a] x is from synthesis.
[b] x is from Rietveld profile fitting ($x = x_L + x_N$) and $\eta = x_L - x_N$.
[c] The sample was fit in the cubic structure. R_B is defined in (6),

$$R_{wp} = \left[\frac{\sum w_i(y_{io}-y_{ic})^2}{\sum w_i y_{io}^2} \right]^{1/2},$$

and w_i is the weight of peak,

$$R_{expt} = \left[\frac{N-P}{\sum w_i y_{io}^2} \right]^{1/2},$$

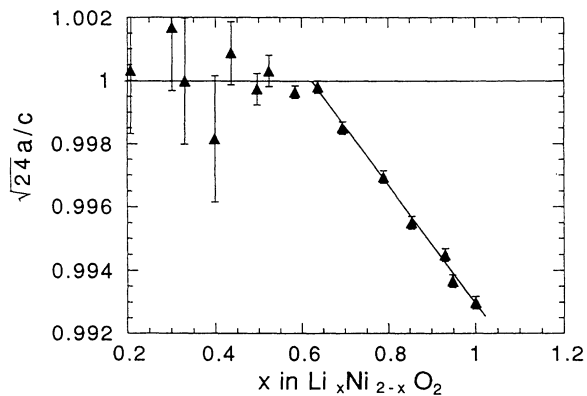where N is the number of observations and P is the number of least-squares parameter being estimated.

FIG. 7. The ratio a_h/c_h multiplied by $\sqrt{24}$ vs "x from Rietveld profile fitting." The structure is cubic for $\sqrt{24}\,a_h/c_h = 1$. The straight line fit to the data for $x > 0.62$ gives $x_C = 0.62 \pm 0.01$.

given by other workers.[2,5] For $x < 0.62$ in the cubic structure, the refined x differ by less than 0.03 between the cubic and the hexagonal structures used in the Rietveld profile fitting. Figure 7 shows $\sqrt{24}\,a_h/c_h$ from Rietveld profile fitting in the hexagonal structure, for $0 \leq x \leq 1$. When $\sqrt{24}\,a_h/c_h = 1$ the structure is cubic. The error bars are larger for $x < 0.62$ than those for $0.62 < x < 1.0$, because fewer Bragg peaks are included in the refinements. In our estimate the composition of the order-disorder transition is best obtained from Fig. 7. We measure $x_c = 0.62 \pm 0.01$.

Figure 8 shows the order parameter η versus "x from synthesis." At $x = 1$, full order is still not obtained since $\eta = 0.96$; this means there are some Li atoms in Ni-rich layers and some Ni atoms in Li-rich layers even for stoichiometric $LiNiO_2$. This result agrees with that from recent neutron-scattering measurements on $LiNiO_2$.[13] For $x < 0.62$, there is still short-range order as evidenced by the weak and broad peaks in the $(003)_H$ position. Our Rietveld refinements are all done in the hexagonal system and do not treat the short-range order peak well. The refinement gives nonzero long-range order parameters
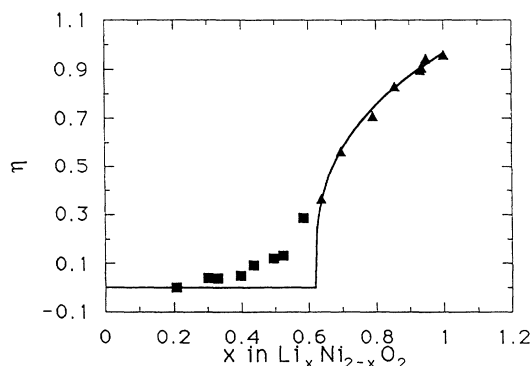
below $x_c = 0.62$ in an attempt to fit the weak broad peak. We have sketched a guide to the eye in Fig. 8 which indicates how the *long-range* order parameter must behave. We have indicated with squares, those fitting results which are an artifact of our procedure and *not* indicative of true long-range order. More careful fitting of the critical scattering is needed to fully understand the short-range order. Before we discuss this short-range order, it is useful to consider a lattice-gas model for $Li_xNi_{2-x}O_2$.

V. LATTICE-GAS MODEL

The system $Li_xNi_{2-x}O_2$ consists of one fcc frame of oxygen and one fcc frame of metal cations. The octahedral interstitial sites of the oxygen lattice are where the cations can be positioned. At each site either a Li atom or a Ni atom can be placed subject to the constraint that we have x Li and $(2-x)$ Ni atoms per formula unit. A lattice-gas model is therefore appropriate for the treatment of this material. Interactions between metal atoms causes the ordered arrangement in the $(111)_C$ planes. Figure 9 shows the structure of the metal frame. There are 12 nearest neighbors (checkerboard circles) and six next-nearest neighbors (grey circles) for each site (black circles). All the six next-nearest neighbors do not share the same $(111)_C$ plane with the site at the origin. However, six of the nearest neighbors share the same $(111)_C$ layer with the atom at the origin and the other six do not.

FIG. 8. The long-range order parameter from Rietveld profile fitting vs "x from Rietveld profile fitting." For $x < 0.62$, the data do not indicate long-range order (see text). The solid line is a guide to the eye.
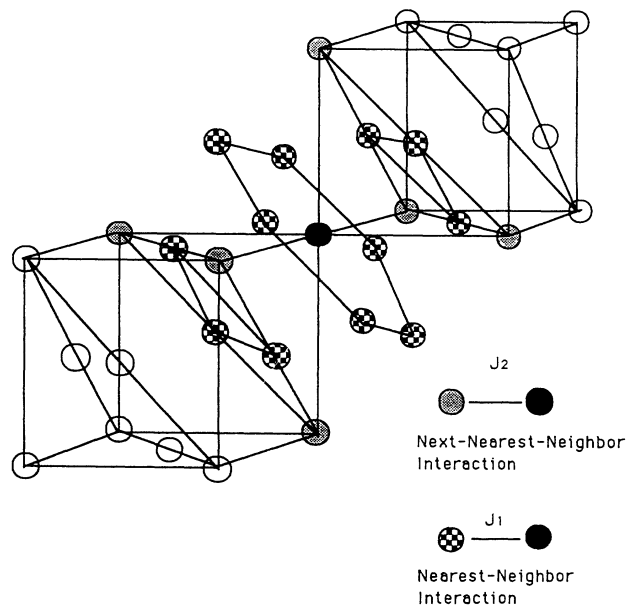

FIG. 9. The cation fcc frame showing the nearest neighbor (checkerboard) and next-nearest neighbors (grey) to a particular site (black). The first- and second-neighbor interaction energies are shown.

In the lattice-gas treatment we assume interactions between pairs of metal cations occupying nearest neighbor (NN) and next-nearest neighbor (NNN) sites and neglect longer-ranged interactions. These are denoted J_1^{NN},

$J_1^{LN} = J_1^{NL}$, J_1^{LL} for Ni-Ni Ni-Li and Li-Li first neighbor interactions, respectively. Next-nearest-neighbor interactions use the same notations, except the subscript 2 replaces the 1. The model Hamiltonian is then

$$H = \mu^L \sum_i x_i + \mu^N \sum_i y_i + \frac{1}{2} \sum_{i,j}^{NN} (J_1^{LL}x_ix_j + J_1^{LN}x_iy_j + J_1^{NL}y_ix_j + J_1^{NN}y_iy_j) + \frac{1}{2} \sum_{i,j}^{NNN} (J_2^{LL}x_ix_j + J_2^{LN}x_iy_j$$
$$+ J_2^{NL}y_ix_j + J_2^{NN}y_iy_j) . \qquad (7)$$

Here, $x_i = 1$ if site i is filled by Li and $x_i = 0$ if site i not filled by Li. $y_i = 1$ if site i is filled by Ni and $y_i = 0$ if site i is filled by Ni. μ^N and μ^L are the chemical potentials for Li and Ni atoms, respectively, and the sums over the interaction terms run over all pairs of nearest-neighbor atoms (the first term) and all pairs of next-nearest-neighbor atoms (the second term).

In our model we assume that all available sites are filled by either Li or Ni and that there are no cation vacancies. This allows considerable simplification of our Hamiltonian, since then $y_i = 1 - x_i$. Making this substitution we obtain

$$H = \sum_i \mu x_i + \frac{1}{2} \sum_{i,j}^{NN} J_1 x_i x_j + \frac{1}{2} \sum_{i,j}^{NNN} J_2 x_i x_j + N\mu^N$$
$$+ 6NJ_1^{NN} + 3N_2^{NN} , \qquad (8a)$$

where

$$\mu = \mu^L - \mu^N + 2(J_1^{LN} - J_1^{NN} + J_2^{LN} - J_2^{NN}) ,$$

$$J_1 = J_1^{LL} + J_1^{NN} - 2J_1^{LN} ,$$

and

$$J_2 = J_2^{LL} + J_2^{NN} - 2J_2^{LN} .$$

Because we can redefine the zero of energy, we drop the constant terms $N\mu^N$, NJ_1^{NN}, and NJ_2^{NN} in our subsequent analysis. Here, x_i is equal to 1 if a site is filled by Li and $x_i = 0$ if it is not. Therefore, we have transformed the Hamiltonian from that commonly seen for A-B alloys to that found for lattice-gas models as is usually done.[14,15]

In order for the $(111)_C$ superlattice ordering to be stabilized it turns out that $J_2 \geq 0.5|J_1|$; for details the reader is referred to Ref. 16. For this case, a Bragg-Williams treatment of the problem is useful which we make below. In the Bragg-Williams model we assume a superlattice structure commensurate with the ordered state. Assuming $(111)_C$ ordering, the Bragg-Williams Hamiltonian (8) is obtained by replacing the site occupancies x_i with

$x + \eta/2$ and $x - \eta/2$ for sites on alternate $(111)_C$ cation planes. Here $x = \langle x_i \rangle$ is the average lithium concentration in the cation sites, equal to x in the compound $Li_xNi_{1-x}O$ and η is the order parameter defined earlier, in Eq. (1).

Making the substitution and doing some algebra we obtain the Bragg-Williams Hamiltonian

$$\frac{H}{N} = \mu x + 3(2J_1 + J_2)x^2 - \frac{3}{4}J_2\eta^2 \qquad (8b)$$

from which one can immediately see that the nearest-neighbor interaction, J_1, does not couple to the order parameter within mean-field theory. Figure 9 shows this as well; distributing 6 Li atoms randomly over the 12 nearest neighbors of a central Li atom "costs" $6J_1$ in energy, the same as if the atoms are in the ordered state, so we do not expect J_1 to couple to this ordered state. The order parameter η is actually fourfold degenerate corresponding to the four cubic directions, [111], [1$\bar{1}$1], [11$\bar{1}$], and [1$\bar{1}$1], with order parameters η_1, η_2, η_3, and η_4, respectively.

Does the system select just one η or some linear combination of all four? To answer this we consider the relative entropies for these two situations. In mean-field theory, entropy is maximized in lattice-gas arrangements with all site occupancies equal to one half, which is not possible in an ordered state with $\eta > 0$. When $\eta \neq 0$, entropy is maximized in ordered states where the magnitude of the deviation from half occupancy, is the same on each site. This certainly is true for our ordered state where alternate (111) planes have average compositions $x + \eta/2$ and $x - \eta/2$. In an ordered state which is a mixture of the four (111) states, the magnitude or absolute value of the deviation of the average occupation from 1/2 will vary from site to site. Hence entropy is maximized in phases corresponding to one of the four possible (111) superlattices and not a mixture. A detailed proof of this is given in the Appendix.

The Bragg-Williams free energy is easily shown to be

$$\frac{F}{N} = \frac{H}{N} - \frac{TS}{N} = \frac{H}{N} + \frac{k_BT}{2}\left\{\left[x + \frac{\eta}{2}\right]\ln\left[x + \frac{\eta}{2}\right] + \left[1 - \left[x + \frac{\eta}{2}\right]\right]\ln\left[-\ln\left[x + \frac{\eta}{2}\right]\right] + \left[x - \frac{\eta}{2}\right]\ln\left[x - \frac{\eta}{2}\right]\right.$$
$$\left. + \left[1 - \left[x - \frac{\eta}{2}\right]\right]\ln\left[1 - \left[x - \frac{\eta}{2}\right]\right]\right\} . \qquad (9a)$$

Expanding in powers of η we obtain

$$\frac{F}{N} = \mu x + 3(2J_1 + J_2)x^2 - \tfrac{3}{4}J_2\eta^2 + k_B T[x\ln x + (1-x)\ln(1-x)] + \frac{k_B T}{8}\left[\frac{1}{x} + \frac{1}{1-x}\right]\eta^2$$

$$+ \frac{k_B T}{192}\left[\frac{1}{x^3} + \frac{1}{(1-x)^3}\right]\eta^4 + \cdots .$$

(9b)

Using the Landau theory of phase transitions we expect that F will be minimized for $\eta = 0$ whenever

$$\frac{k_B T}{2}\left[\frac{1}{x} + \frac{1}{1-x}\right] - 3J_2 > 0$$

(9c)

and that F will be minimized for $\eta > 0$ whenever

$$\frac{k_B T}{2}\left[\frac{1}{x} + \frac{1}{1-x}\right] - 3J_2 < 0 .$$

(9d)

This phase transition to $\eta \neq 0$ occurs in the Bragg-Williams treatment when equality holds above, giving

$$x_c(1 - x_c) = \frac{k_B T}{6J_2} ,$$

(9e)

where x_c is the critical lithium concentration in $Li_x Ni_{1-x}O$ beyond which ordering in $(111)_C$ planes occurs. The data in Fig. 8 show that the ordered state disappears for $x < x_c \approx 0.62$ in $Li_x Ni_{2-x}O_2$ which corresponds to $x_c = 0.31$ in $Li_x Ni_{1-x}O$. Substituting $x_c = 0.31$ into the above equation gives
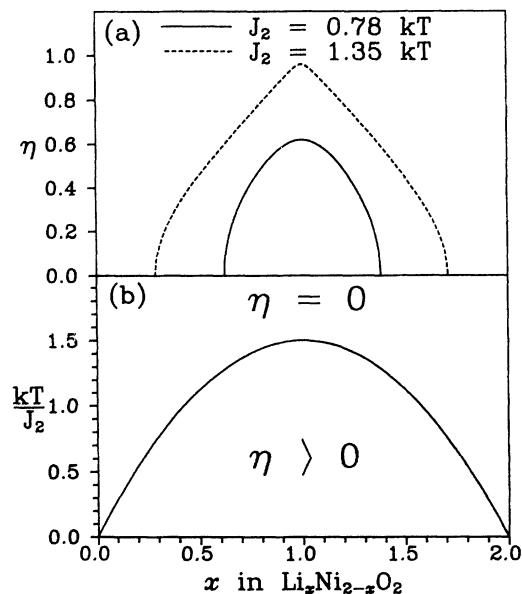
$$\frac{J_2}{k_B T} = 0.78 .$$

(9f)

FIG. 10. (a) The order parameter vs x calculated by the Bragg-Williams model for the values of $J_2/k_B T$ shown and $J_1 = 0$. (b) The order-disorder phase diagram calculated using the Bragg-Williams model for $J_1 = 0$.

Figure 10(a) shows η versus x in $Li_x Ni_{2-x}O_2$ for $J_2/(k_B T) = 0.78$ (chosen so that x_c agrees with the data) and for $J_2/(k_B T) = 1.35$ (chosen so that the maximum in η agrees with the data) calculated by minimizing the Bragg-Williams free energy given by Eq. (9a) with respect to η. This can be directly compared to the data in Fig. 8. The agreement is encouraging and suggests that better solutions to the statistical mechanics, such as Monte Carlo methods, are in order. Figure 10(b) shows the mean-field phase diagram for the model.

VI. MONTE CARLO RESULTS

Here we use the Monte Carlo method to calculate the order parameter versus x and T. The Metropolis method[17] is used to get the equilibrium ensembles of the system described by the Hamiltonian in Eq. (8a). The calculation uses an fcc lattice of cation sites and periodic boundary conditions. As order develops we do not know a priori along which of the four equivalent cubic directions $[1\,1\,1]$, $[1\,\bar{1}\,1]$, $1\,1\,\bar{1}]$, or $[1\,\bar{1}\,\bar{1}]$ the order develops. To calculate the long-range order parameter we calculate the average site occupancy in layers normal to $[1\,1\,1]$ and then take the difference between the average occupancies of the set of alternate planes. This we call η_1. We repeat this procedure for planes normal to the $[1\,\bar{1}\,1]$, $[1\,1\,\bar{1}]$, and $[1\,\bar{1}\,\bar{1}]$ directions, finding η_2, η_3, and η_4, respectively. In the ordered state, only one of the four order parameters is significantly different from zero. The overall order parameter η is then defined to be

$$\eta = (\eta_1^2 + \eta_2^2 + \eta_3^2 + \eta_4^2)^{1/2}$$

(10a)

to ensure that our computation is sensitive to the development of long-range order in any of the four possible directions and to ensure that η is positive. The fcc lattice has four atoms per unit cell. Our lattices ranged in size from a $4\times4\times4$ unit cell to a $12\times12\times12$ cell or from 256 atoms to 6912 atoms.

Figure 11 shows η and x in $Li_x Ni_{2-x}O_2$ calculated for $J_2 = 1.2k_B T$, and $J_1 = -0.5k_B T$ for a variety of lattice sizes. We examine the effect of the choice of J_1 below. At $x = 1$, when the lattice is half filled by Li, the order parameter reaches a maximum of 0.92, which is approximately independent of lattice size. However, the order parameter depends on the lattice size near the critical composition, x_c. The finite-sized lattice we use shows residual order below x_c which decreases as the lattice size increases. Figure 12 shows $\langle \eta \rangle$ versus x for $J_2 = 1.35k_B T$ with $J_1 = -0.5k_B T$ calculated by Monte Carlo $(L = 12)$ and mean-field theories for $J_2 = 1.35k_B T$ and $J_2 = 0.78k_B T$. We cannot fit the experiment using
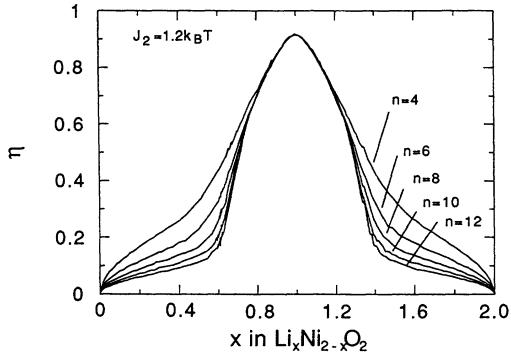
FIG. 11. The order parameter η from the Monte Carlo calculations for various lattice sizes and a fixed next-nearest-neighbor interaction constant. The results are averaged over 1000 equilibrium ensemble and $J_1 = -0.5k_BT$.

mean-field theory at both $x = x_c$ and $x = 1$ with the same J_2.

The data in Fig. 7 suggest that experimentally $x_c = 0.62$ and the data in Fig. 8 show that the maximum in η at $x = 1$ is $\eta_{max} = 0.96$. Figure 12 also shows our attempt to fit the data with the Monte Carlo calculation using $J_2 = 1.35k_BT$ and $J_1 = -0.5k_BT$ on the largest $(12 \times 12 \times 12)$ lattice size considered. The fit is excellent in the ordered state which shows that $Li_xNi_{2-x}O_2$ can be well described by a lattice-gas model. Figure 13 shows the effects of the choice of J_1 on the results for $-0.5k_BT \leq J_1 \leq 2.0k_BT$. For fixed J_2, increasing $|J_1|$ reduces the extent of the ordered phase, but the reduction is very minor for $|J_1| < J_2/2$. As Fig. 13 shows, the three curves for η versus x for $J_1/k_BT = -0.5$, 0.0, 0.5 with $J_2 = 1.35k_BT$ are almost identical. Only when $|J_1| > J_2/2$ does the behavior of η vs x deviate significantly, affecting the value of x_C, much more strongly than η_{max}. Although we could increase the value of J_2 for $J_1 = 1.0k_BT$ to obtain agreement with the data at x_C, this would affect the agreement between the predicted and observed values of η_{max} at $x = 1$ in
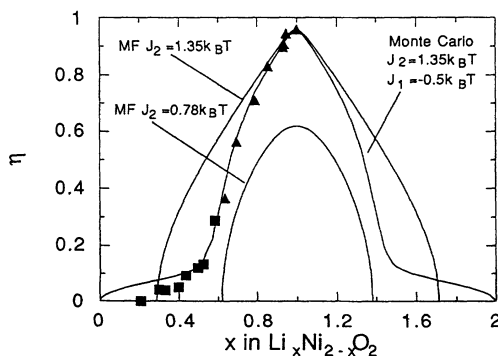

FIG. 12. Order parameter η vs x in $Li_xNi_{2-x}O_2$. The solid points are the data from Fig. 8 and the curves are from the Monte Carlo simulation $(L = 12, J_1 = -0.5k_BT)$ and the mean-field theory.
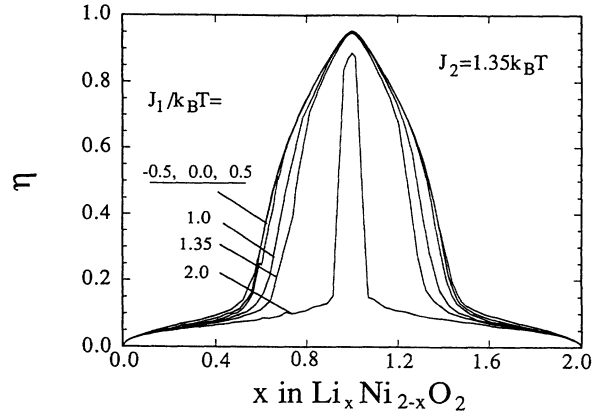

FIG. 13. Order parameter η vs x in $Li_xNi_{2-x}O_2$ for $J_2 = 1.35k_BT$ and various J_1/k_BT (-0.5, 0.0, 0.5, 1.0, 1.35, 2.0). For $-0.5k_BTJ_1 < 1.0k_BT x_c$ is rather insensitive to J_1.

$Li_xNi_{2-x}O_2$. When $|J_1| \cong 2J_2$ the [1 1 1] ordering is severely affected as shown by the curve in Fig. 13 for $J_1 = 2.0k_BT$, $J_2 = 1.35k_BT$. This result is consistent with earlier work.[17] When $J_1 < -0.5k_BT$, the phase transition to the ordered phase becomes clearly first order in the Monte Carlo calculations (at $J_1 = -0.5k_BT$ it is hard to tell whether the transition is continuous or weakly first order; for $J_1 > 0$, the transition is clearly continuous). A region of coexisting phases is observed near the transition point for $J_1 = -1.0k_BT$. That is, a coexistence between a disordered phase with composition, x_1, and an ordered phase with composition, x_2, occurs for $x_1 \leq x \leq x_2$. This is consistent with experiment and therefore we feel that J_1 is most likely positive.

These results clearly suggest that J_2 is larger than J_1 in this material. This is somewhat surprising since the cation-cation bond length corresponding to J_2 is $\sqrt{2}$ times that corresponding to J_1 and usually interaction strengths decrease with distance. The interactions J_1 and J_2 are made up of Li-Li, Ni-Ni, and Li-NI interactions as given in Eq. (8a). Each of these interactions is very complicated to estimate.

The critical composition, x_c, where order develops, is most easily determined by plotting the fluctuations of the order parameter

$$N(\langle \eta^2 \rangle - \langle \eta \rangle^2) \tag{10b}$$

versus x. Noise-free fluctuation quantities such as $\langle \eta^2 \rangle - \langle \eta \rangle^2$ are very difficult to calculate with conventional Monte Carlo methods, particularly if successive spin configurations are highly correlated (autocorrelation). In order to alleviate this problem we have used Ferrenberg and Swendsen's *multihistogram* method[18] which allows optimal use of all the simulation data.

The probability distribution at chemical potential μ, $P_\mu(x)$, is generated by building a histogram of the number of lattice-gas configurations that have x in the range x_i and $x_i + \Delta x$, where i labels a bin in the histogram and Δx is the bin size. In this work we used $\Delta x = 4 \times 10^{-5}$. From the reweighting transformation

$$P_{\mu'}(x) = \frac{P_\mu(x)\exp[-\beta x(\mu'-\mu)]}{\sum_x P_\mu(x)\exp[-\beta x(\mu'-\mu)]} \quad (10c)$$

one can see that the exact probability distribution at μ actually contains all the necessary information needed to calculate $P_{\mu'}(x)$ for any other chemical potential μ'. In practice $P_\mu(x)$ only contains information on distributions for μ' near μ, due to poor counting statistics in the wings of the histogram far from $\langle x \rangle_\mu$. However, data quality can be improved considerably by combining numerous histograms generated at different μ's.

In order to obtain an accurate estimate of x_c we have calculated the following three fluctuation quantities:

$$N(\langle \eta^2 \rangle - \langle \eta \rangle^2) , \quad (11a)$$

$$N(\langle x^2 \rangle - \langle x \rangle^2) , \quad (11b)$$

$$N(\langle x\eta \rangle - \langle x \rangle \langle \eta \rangle) , \quad (11c)$$

which all have maxima at the phase transition. Figure 14(a) shows the fluctuations in the order parameter η for three different lattice sizes, $L = 4$, 8, and 12. Two other lattice sizes, $L = 6$ and 10 (not shown) were also simulated. The solid lines in Fig. 14(a) are calculated using the
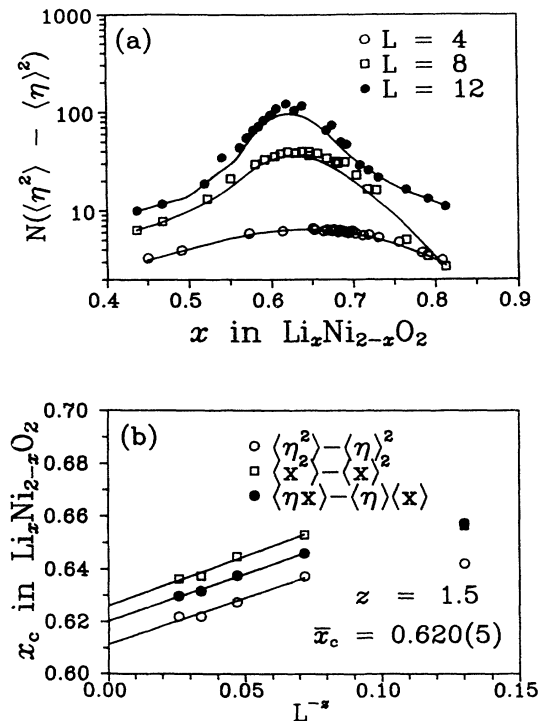

FIG. 14. (a) The fluctuations in the order parameter calculated from Monte Carlo averages (data points) and the multihistogram method (solid lines) for three lattice sizes. Averages and histograms generated from 10 000 Monte Carlo steps at equilibrium for $J_2 = 1.35k_BT$ and $J_1 = -0.5k_BT$. (b) Power-law (see text) extrapolation of x_c to infinite lattice size giving an average $\bar{x}_c = 0.620(5)$. x_c's for finite lattice sizes were calculated from three fluctuation quantities that all have maxima at the phase transition.

multiple histogram method and discrete data points are obtained by standard averaging at each μ simulated. For each μ, 1000 MCS were allowed for the system to reach equilibrium and a further 10 000 MCS for averaging of thermodynamic quantities. In order to estimate x_c in the thermodynamic limit we have extrapolated assuming a power-law dependence on lattice size

$$x_c(L) = x_c(\infty) + AL^{-z} . \quad (12)$$

The fits [Fig. 14(b)] were rather insensitive to the exponent z but the best results were obtained for $z = 1.5$ giving three x_c values 0.612 ($\langle \eta^2 \rangle - \langle \eta \rangle^2$), 0.627 ($\langle x^2 \rangle - \langle x \rangle^2$), and 0.6208 ($\langle \eta x \rangle - \langle \eta \rangle \langle x \rangle$) with an average $\bar{x}_c = 0.620(5)$.

VII. SHORT-RANGE ORDER

Figure 15 shows the $(003)_H$ Bragg peak region measured at several values of x in $Li_xNi_{2-x}O_2$. The data are displayed with different intensity scales, but this does not affect the peak shape. As x decreases below $x = 0.62$, the width of the peak increases rapidly. The broad weak peak indicates the presence of short-range order, the precursor to the long-range order which develops for $x > 0.62$. This short-range represents the tendency of Li atoms to avoid simultaneously filling next-nearest-neighbor sites. Detailed analysis of the short-range order will be presented elsewhere.

VIII. DISCUSSION

We have shown that the order-disorder transition in $Li_xNi_{2-x}O_2$ is well modeled with a lattice-gas treatment. Our model reproduces the data very well using $J_2 = 1.35k_BT$ with a wide range of $J_1(-0.5k_BT < J_1 < 0.5k_BT)$. It remains to determine the value of T. In our opinion, the temperature of importance is the temperature at which the Ni atoms can no longer move. For the lattice-gas treatment to be reasonable, both Li and Ni must be mobile and diffusing freely from site to site.
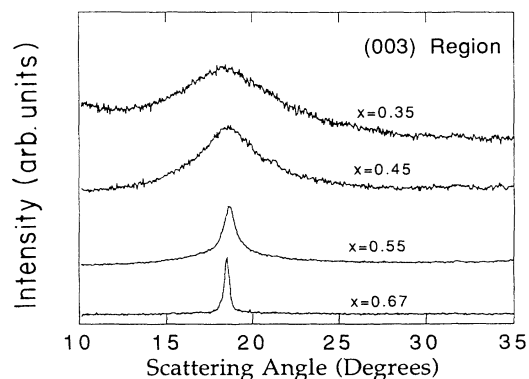

FIG. 15. X-ray diffraction shows the short-range order in $Li_xNi_{2-x}O_2$ for $0 \le x \le 0.62$. The Bragg peak in the $(003)_H$ region has been multiplied by a scale factor which increases as x decreases to make the peak visible at low x.

During cooling of our samples the Ni atoms freeze at some temperature; [probably around 600 °C since synthesis of $LiNiO_2$ is very slow (> 40 h) at this temperature] thus our samples are instantaneous records of the equilibrium that existed just above that temperature. Using $T = 600$ °C, we calculate $J_2 = 0.11$ eV. Preliminary high-temperature diffraction measurements using an *in situ* furnace show that the ordered phase in $Li_{0.66}Ni_{1.34}O_2$ is reversibly suppressed at about 1000 °C, consistent with our estimate of T above. Further high-temperature work is in progress.

One goal of our research is to extract the cation-cation interacalation energies so that we can model the behavior of $Li\text{-}Li_xNiO_2$ interaction batteries with lattice-gas models as has been done previously for other intercalation compounds.[19,20] Unfortunately, we have shown that the value of the nearest-neighbor interaction, most important for that application, cannot be determined from the order-disorder in $Li_xNi_{2-x}O_2$ since the nearest-neighbor interaction is not sensitive to the observed order parameter for this materials. Other measurements, such as the variation of the Li chemical potentials in $Li_xNi_{2-x}O_2$ with x are needed to determine the Li-Li contribution to J_1.

The Li transition-metal oxides ($LiMO_2$) show a rich variety of structures based on close packed oxygen layers.[21] The Li and M atoms form a variety of ordered arrangements which can probably be explained by suitable choices of cation-cation interaction energies in a lattice-gas formalism. One of our goals is to determine a set of interactions consistent with the observed structures.

APPENDIX

In order to prove that entropy is maximized when only one of the four degenerate order parameters η_1, η_2, η_3, or η_4 is selected, we must write the general site occupancy as

$$x_i = x + \frac{1}{2} \sum_{\alpha=1}^{8} \eta_{q_\alpha} \exp(i q_\alpha \cdot r_i) , \tag{A1}$$

where x is the uniform site occupation. r_i is the lattice vector for site i, and the q_α are the eight ordering wave vectors, $q_1 = (1,1,1)$, $q_2 = (1,\bar{1},\bar{1})$, $q_3 = (\bar{1},1,\bar{1})$, $q_4 = (\bar{1},\bar{1},1)$, $q_5 = -q_1$, $q_6 = -q_2$, $q_7 = -q_3$, and $q_8 = -q_4$.

Reality of the x_i implies the following constraint:

$$\eta_{q_\alpha} = \eta^*_{-q_\alpha} . \tag{A2}$$

Thus $\eta_{q_1} = \eta^*_{q_5}$ and we define $\eta_1 = \eta_{q_1} + \eta^*_{q_5}$ with similar relationships for the other three order parameters. Substituting (A1) into the Landau expansion (7) we obtain

$$F/N = \mu x + 3(2J_1 + J_2)x^2$$
$$+ \left[\frac{k_B T}{8} \frac{1}{x(1-x)} - \frac{3}{4}J_2 \right](\eta_1^2 + \eta_2^2 + \eta_3^2 + \eta_4^2)$$
$$+ \frac{k_B T}{192} \left[\frac{1}{x^3} + \frac{1}{(1-x)^3} \right] f^{(4)} , \tag{A3}$$

where

$$f^{(4)} = \sum_{\alpha,\beta,\gamma,\varepsilon} \eta_\alpha \eta_\beta \eta_\gamma \eta_\varepsilon \delta(q_\alpha + q_\beta + q_\gamma + q_\varepsilon) , \tag{A4}$$

where $\delta(q_\alpha + q_\beta + q_\gamma + q_\varepsilon)$ is a discrete delta function. Expanding the fourth-order term (A4) we have

$$f^{(4)} = 24 \left[\sum_\alpha \eta_\alpha^4 + 3 \sum_{\alpha \neq \beta} \eta_\alpha^2 \eta_\beta^2 + 2\eta_1 \eta_2 \eta_3 \eta_4 \right] \tag{A5}$$

$$= 24 \left[3 \left[\sum_\alpha \eta_\alpha^2 \right]^2 - 2 \sum_\alpha \eta_\alpha^4 + 2\eta_1 \eta_2 \eta_3 \eta_4 \right] \tag{A6}$$

which determines whether or not one η_α is selected. In order to make a meaningful comparison of free energies, the values of the η_α must be chosen so as to satisfy

$$\eta_1^2 + \eta_2^2 + \eta_3^2 + \eta_4^2 = \eta^2 . \tag{A7}$$

For simplicity we will test the two extreme cases for which (A7) is satisfied.

Case 1: $\eta_1 = \eta_2 = \eta_3 = \eta_4 = \dfrac{\eta}{2}$:

$$f^4 = 24(3\eta^4 - \tfrac{1}{2}\eta^4 + \tfrac{1}{8}\eta^4) = 63\eta^4 . \tag{A8}$$

Case 2: $\eta_1 = \eta$, $\eta_2 = \eta_3 = \eta_4 = 0$:

$$f^4 = 24(3\eta^4 - 2\eta^4) = 24\eta^4 . \tag{A9}$$

Since the coefficient of the fourth-order term is positive definite and (A9) < (A8), the free energy is minimized for case 2 to over case 1, i.e., only *one* of the four η's will be selected.

[1]L. D. Dyer, B. S. Borie, and G. P. Smith, J. Am. Chem. Soc. 78, 1499 (1954).

[2]J. B. Goodenough, D. G. Wickham, and W. J. Croft, J. Phys. Chem. Solids 5, 107 (1958).

[3]J. B. Goodenough, D. G. Wickham, and W. J. Croft, J. Appl. Phys. 29, 382 (1958).

[4] V. W. Bronger, H. Bade, and W. Klemm, Z. Anorg. Allg. Chem. 333, 188 (1964).

[5]J. R. Dahn, Ulrich von Sacken, and C. A. Michal, Solid State Ionics 44, 87 (1990).

[6]J. R. Dahn, U. Von Sacken, M. W. Juzkow, and H. Al-Janaby, J. Electrochem. Soc. 138, 2207 (1991).

[7]H. M. Rietveld, J. Appl. Crystallogr. 2, 65 (1969).

[8]J. C. Taylor, Aust. J. Phys. 38, 519 (1985).

[9]R. J. Hill and C. J. Howard, J. Appl. Cryst. 18, 173 (1985).

[10]R. J. Hill and I. C. Madsen, J. Appl. Cryst. 19, 10 (1986).

[11]C. J. Howard, J. Appl. Cryst. 15, 615 (1982).

[12]R. J. Hill and C. J. Howard, Program for Rietveld Analysis of Fixed Wavelength X-ray and Neutron Powder Diffraction Patterns–Version LHPM1, AAEC (Lucas Heights Research Laboratories N.S.W., Australia) (unpublished).

[13]J. N. Reimers, J. R. Dahn, J. E. Greedan, C. V. Stager, G. Liu, I. Davidson, and U. von Sacken (unpublished).

[14]J. M. Ziman, *Models of Disorder* (Cambridge University Press,

New York, 1979).

[15]B. E. Warren, *X-Ray Diffraction* (Addison-Wesley, New York, 1969).

[16]J. S. Grant, *Effective Field Theories of Magnetism* (Saunders, Philadelphia, PA, 1966).

[17]K. Binder, *Monte Carlo Method in Statistical Physics* (Springer-Verlag, Berlin, 1986).

[18]A. M. Ferrenberg and R. H. Swendsen, Phys. Rev. Lett. **61**, 2635 (1988); **63**, 1195 (1989); Comput. Phys. **3**(5), 101 (1989).

[19]S. T. Coleman, W. R. McKinnon, and J. R. Dahn, Phys. Rev. B **29**, 4147 (1984).

[20]J. R. Dahn and W. R. McKinnon, J. Phys. C **17**, 1423 (1984).

[21]T. A. Hewston and B. L. Chamberland, J. Phys. Chem. Solids **48**, 97 (1987).
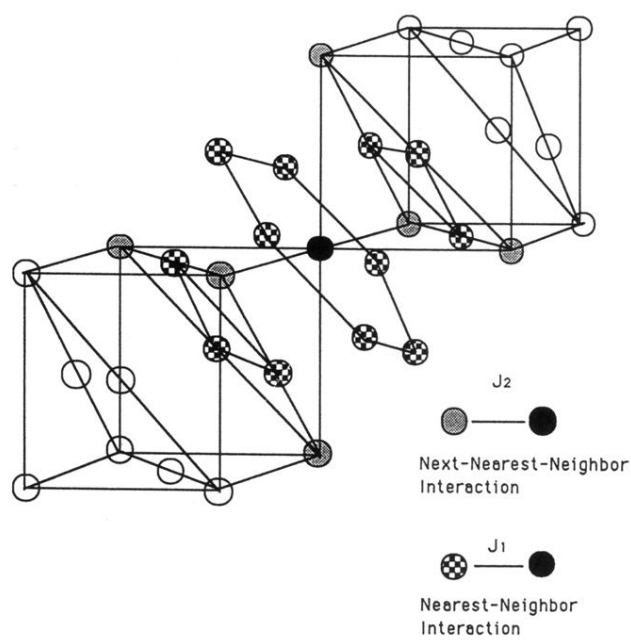
FIG. 9. The cation fcc frame showing the nearest neighbor (checkerboard) and next-nearest neighbors (grey) to a particular site (black). The first- and second-neighbor interaction energies are shown.